ACS APPLIED MATERIALS & INTERFACES

Research Article

www.acsami.org

Tuning Acid–Base Properties Using Mg–Al Oxide Atomic Layer Deposition

David H. K. Jackson,[†,‡] Brandon J. O'Neill,[‡,§] Jechan Lee,[‡,∥] George W. Huber,[‡] James A. Dumesic,[‡] and Thomas F. Kuech*[,†,‡]

[†]Materials Science Program, and [‡]Department of Chemical and Biological Engineering, University of Wisconsin − Madison, Madison, Wisconsin 53706, United States

Supporting Information

ABSTRACT: Atomic layer deposition (ALD) was used to coat γ-Al_2O_3 particles with oxide films of varying Mg/Al atomic ratios, which resulted in systematic variation of the acid and base site areal densities. Variation of Mg/Al also affected morphological features such as crystalline phase, pore size distribution, and base site proximity. Areal base site density increased with increasing Mg content, while acid site density went through a maximum with a similar number of Mg and Al atoms in the coating. This behavior leads to nonlinearity in the relationship between Mg/Al and acid/base site ratio. The physical and chemical properties were elucidated using scanning electron microscopy (SEM), energy-dispersive X-ray spectroscopy (EDS), powder X-ray diffraction (XRD), X-ray photoelectron spectroscopy (XPS), N_2 physisorption, and CO_2 and NH_3 temperature-programmed desorption (TPD). Fluorescence emission spectroscopy of samples grafted with 1-pyrenebutyric acid (PBA) was used for analysis of base site proximity. The degree of base site clustering was correlated to acid site density. Catalytic activity in the self-condensation of acetone was dependent on sample base site density and independent of acid site density.

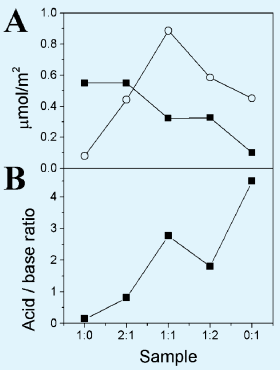

KEYWORDS: *solid base, atomic layer deposition, magnesium aluminum oxide, gamma alumina, acetone self-condensation, pyrene butyric acid*

INTRODUCTION

The use of atomic layer deposition (ALD) in catalysis has found multiple successful applications in recent years.[1−4] ALD is a thin film coating technique known for its excellent conformality in complex geometries and subnanometer-level thickness control.[5] These qualities make ALD well suited for coating the high surface area supports with an active phase to make catalysts or protect deposited nanoparticles. However, few examples exist where the high degree of compositional control offered by ALD has been utilized for catalysis.[4,6,7] We show here that by modifying pulse sequences in the ALD coating of Mg–Al oxide onto γ-Al_2O_3, the surface acid/base properties of a catalyst can be controlled through atomic control of the resulting film composition.

ALD utilizes sequential pulsing of vapor phase precursors that undergo complementary, self-saturating surface reactions. Precursor pulses are separated by inert gas purges or by evacuation of the reactor volume to prevent vapor phase mixing of precursors.

ALD is well studied for the coating of planar substrates, while its application to powders is still a developing area of investigation. Depositions on powder quantities larger than a few grams must be performed using agitation of the particles to increase the diffusion rates of precursor gases through the powder bed. In this study, a fluidized bed reactor was used to provide agitation to the particles,[2,3,6,8,9] in which an inert gas stream was passed upward through a bed of substrate particles supported on a porous distribution plate. At an inert gas velocity above a minimum velocity u_{min}, the particle bed converts to a fluid-like phase, and gas transport through the bed increases dramatically. Fluidized bed ALD was developed by research groups in Boulder[10,11] and Delft.[12]

The use of ALD grown mixed oxide catalysts has been studied in the deposition of Ti–V–O, in which control over the pulsing sequence enabled optimization in the liquid phase epoxidation of cyclohexene.[13] ALD has also been shown to enable the tailoring of catalyst activity,[14] although, to the best of our knowledge, this is the first example of using ALD to tune both acidity and basicity.

Basic oxides have been studied for their use as catalysts and catalyst supports.[15,16] Traditionally, solid bases have been made by precipitation of the bulk oxide, ion exchange with alkali metal cations,[17,18] impregnation or occlusion with basic salts or metals,[19] and nitridation.[20] These heterogeneous oxides are of interest in catalysis because of their potential to replace corrosive homogeneous catalysts such as NaOH, facilitate catalyst separation, and reduce waste stream processing. Basic oxide catalysts have been used in numerous chemistries including isomerization of alkenes, addition reactions, Knoevenagel condensations, and aldol condensations.[17,21] They are also relevant in biomass conversion strategies, and have been used for the aldol condensation of furfurals with acetone and

Received: May 12, 2015
Accepted: July 13, 2015
Published: July 13, 2015

DOI: 10.1021/acsami.5b04107
ACS Appl. Mater. Interfaces 2015, 7, 16573−16580

propanal to produce diesel fuel precursors.[22] We have selected mixed Mg−Al oxide for study here due to its widespread use as a basic oxide.[15]

Magnesium oxide (MgO) films have been deposited by ALD onto planar Si and soda lime glass using Cp_2Mg (bis(cyclopentadienyl)magnesium) and water.[23] Also, magnesium aluminate and mixed magnesium aluminum oxide films have been deposited by using a similar MgO ALD process in combination with Al_2O_3 ALD using trimethylaluminum (TMA).[6,24] In addition to Cp_2Mg, bis(ethylcyclopentadienyl)-magnesium ($EtCp_2Mg$)[25] and $Mg(thd)_2$ (thd = 2,2,6,6-tetramethyl-3,5-heptanedione)[26] have been studied in the ALD of MgO. We have selected Cp_2Mg, TMA, and H_2O as precursors here in the ALD of Mg−Al oxide. As a powder substrate, we have used γ-Al_2O_3, due to its broad usage and characterization in the field of catalysis.

EXPERIMENTAL SECTION

ALD was performed in a home-built fluidized bed reactor described previously.[9,10] Briefly, the deposition chamber consists of a vertical stainless steel tube 45 cm tall, 5 cm in diameter at the bottom, and flared out at the middle and top to 9 cm. The chamber is lined with a removable insert that has a porous (10 μm) stainless steel distribution plate at the bottom to support the powder bed. Argon was used as a carrier gas at a flow of 30 cm^3(STP)/min, with the reactor pressure varied between 3 and 7 Torr during depositions. TMA (97%, Sigma-Aldrich) was held in a cylinder at room temperature and fed through a metering valve to control the flow. Cp_2Mg (99.9% Strem) was held in a bubbler at 100 °C, with the 30-sccm argon carrier stream diverted through the bubbler to entrain the precursor. Deionized water was held in a cooling bath at 12 °C. Depositions were performed at a reactor temperature of 200 °C. Mg and Al precursors were alternated with water pulses, and all pulses were followed by 10 min purges. The γ-Al_2O_3 (Strem, low soda) substrate was prepared by crushing pellets in a mortar and pestle, with the resulting powder sieved to be within the size range of 11−30 μm. Each deposition was performed on 1 g of γ-Al_2O_3 powder. Pulse lengths were determined using a mass spectrometer downstream of the reaction chamber monitoring the reaction byproducts. A pair of complementary precursor pulses is considered a single ALD cycle. The two types of cycles used here are Cp_2Mg−H_2O and TMA−H_2O. All samples were coated using 36 ALD cycles; however, the supercycles were varied. A supercycle is a repeated pattern of cycles, such as 2 × (Cp_2Mg−H_2O) + 1 × (TMA−H_2O). This supercycle would be denoted 2:1, where the numbers represent the Mg/Al pulse ratio.

Scanning electron microscopy (SEM) and energy dispersive X-ray spectroscopy (EDS) were performed on a Zeiss LEO-1530 scanning electron microscope equipped with silicon drift detector. Fifteen points were analyzed for each sample, with an accelerating voltage of 10 kV.

X-ray diffraction (XRD) measurements in a θ−2θ geometry were performed on a Bruker D8 Discovery using a Cu Kα source.

X-ray photoelectron spectroscopy (XPS) was performed with an Al Kα source and a hemispherical electron energy analyzer using a Thermo K-alpha instrument. Measurements were carried out at room temperature at an instrument base pressure of ~1×10^{-9} Torr. XPS scans were acquired using a 30° takeoff angle for the Al 2p, Mg 2p, C 1s, and O 1s spectral regions with 50 eV pass energy. Adventitious carbon at 284.8 eV of the C 1s peak was used as an internal standard.

Calcination of samples was carried out at 600 °C for 2 h in air. Except for in the case of XRD, calcined samples were stored under argon prior to use to prevent reaction with CO_2 in the atmosphere.

Surface areas were measured using the Brunauer-Emmett-Teller (BET) equation from N_2 physisorption data at −196 °C obtained using a Micromeritics ASAP 2020 system. Barret−Joyner−Halenda (BJH) desorption was used to estimate pore volume distributions. Before N_2 physisorption, the samples were degassed under vacuum at 200 °C.

1-Pyrenebutyric acid (PBA) was grafted onto sample surfaces by treating 200 mg of calcined powder with 25 mg of PBA, and stirring in toluene for 2 days at 70 °C. After grafting, the powder was washed with toluene and then tetrahydrofuran (THF) to remove remaining, nongrafted PBA. Fluorescence emission measurements on PBA grafted powders were performed on a Shimadzu RF-1501 spectrofluorophotometer using an excitation wavelength of 300 nm. Powders were pressed into a mesh and sealed in a cuvette under Ar, and measurements were taken using a front-angle geometry.[27]

Acid- and base-specific surface site densities were determined using temperature-programmed desorption (TPD) of chemisorbed NH_3 and CO_2, respectively. Samples were treated in air at 600 °C for 2 h. After calcination, the sample was cooled under He (Airgas). Next, the flow was changed to 1% NH_3 in He and held at 200 °C or 300 ppm of CO_2 in He and held at room temperature. Following saturation of the surface, the catalyst was degassed in He to remove weakly bound physisorbed species from the surface. The reaction of acid sites with NH_3 at 200 °C and CO_2 with base sites at room temperature led to irreversible chemisorption of the probe molecule to the surface of the oxide. The surface stoichiometry for adsorbents and reactive sites was defined as 1:1. During a temperature ramp in He, the amounts of NH_3 and CO_2 desorbed from the surface were quantified by measuring the outlet flow rate and measuring the outlet composition using a mass spectrometer (OmniStar, Pfeiffer Vacuum Systems) with a Faraday cup and secondary electron multiplier. Standard deviations in these data were ±4%, a value smaller than the symbols used to represent points in the figure. All reported base site densities reported are areal base site densities, and are calculated using the measured specific surface areas of the samples.

Catalytic reactions were performed in glass reactors stirred at 60 °C in neat acetone. A typical reaction contained 3 mL of acetone and 25 mg of catalyst freshly calcined at 600 °C. Reaction products were quantified using liquid analysis performed on a Shimadzu GC-2010 with an Agilent DB-5MS-UI column. Turnover frequency (TOF) was calculated using values at 1 h of reaction time, with the following equation:

$$\mathrm{TOF} = \frac{(\text{mmol diacetone alcohol})}{(\text{mmol base sites})*(\text{reaction time})}$$

RESULTS AND DISCUSSION

Commercial γ-Al_2O_3 particles were used as a substrate, which were fabricated through the calcination of boehmite. The structure of γ-Al_2O_3 made using this process is well characterized, and is typically described as having a cubic lattice with a tetragonal distortion.[28] The pores of γ-Al_2O_3 form from the breakdown of hydroxide layers of boehmite, and as a result contain most of the hydrogen-containing water and hydroxide species, as well as containing some amorphous regions near the surface.[28]

Particles were coated using 36 ALD cycles with varying Mg/Al pulse ratios. Figure 1 shows SEM images of the substrate particles (Figure 1A) and the 1:0 coated particles after 600 °C

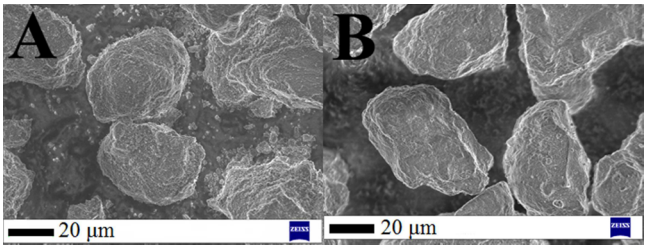

Figure 1. SEM micrograph showing (A) the γ-Al_2O_3 substrate and (B) the 1:0 sample after calcination. The scale bars show 20 μm.

DOI: 10.1021/acsami.5b04107
ACS Appl. Mater. Interfaces 2015, 7, 16573−16580

calcination (Figure 1B). All particles were sieved to within ~11−30 μm in size, which was confirmed by SEM. All samples appeared similar using SEM, demonstrating the ability of ALD to deposit thin, conformal films.

EDS was used to measure the bulk elemental composition of the samples, shown in Figure 2A. Figure 2A shows that

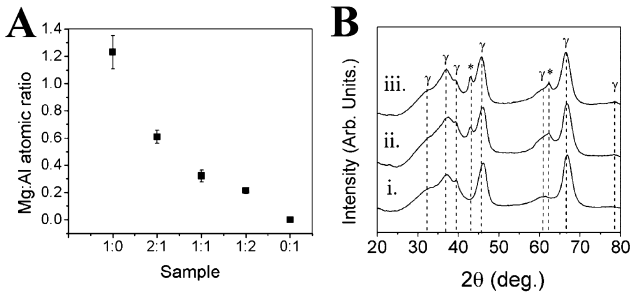

Figure 2. (A) Mg:Al atomic ratio as determined by EDS point analysis. Samples are named *X*:*Y* to reflect the Mg to Al pulse ratio used during ALD. (B) Powder XRD spectra showing (i) uncoated γ-Al_2O_3, (ii) 1:0 as-deposited, and (iii) 1:0 after 600 °C calcination in air. Peaks marked with "γ" indicate γ-Al_2O_3 and "*" indicate cubic MgO.

decreasing Mg/Al pulse ratio resulted in decreasing Mg/Al atomic ratio. Both the γ-Al_2O_3 substrate and the ALD coating are measured due to the sampling depth of this technique being about 10−20 μm, such that this technique cannot be used to directly measure the Mg/Al content of the ALD film. XPS analysis was used to quantify the elemental composition of the samples within the sampling volume of the instrument (typically to a depth of several nm). Similar trends in Mg/Al atomic ratio were observed; however, overall the values were much higher, with 1:0 having an atomic ratio of 7.32 ± 0.75, shown in Supporting Information Figure S1. Additionally, ALD studies on other substrates would allow clearer insight into the chemical species present; however, the composition of low cycle ALD films is extremely surface dependent, and results would vary depending on the substrate.

It should be noted that 1 g of powder in a 5 cm column leads to a bed height of less than 1 mm, leading to difficulties in fluidization; additionally particles in the 10s of micrometers in size are classified as Geldart C particles,[29] which also are known to agglomerate and are difficult to fluidize. The homogeneity of particles was confirmed using EDS, and error bars shown represent sampling of 12−15 particles per experimental sample, and show good homogeneity.

We note that ALD of 36 cycles of either oxide or a mixture of oxides is estimated to completely fill all pores of the γ-Al_2O_3, because the predicted thickness of the oxides (~4 nm)[24] is thicker than the average radius of the pores (~3 nm, BJH). However, the magnesium content in the 1:0 sample was ~2 times lower than that calculated assuming that the entire pore volume was filled with crystalline MgO (Mg/Al ~2.2 for crystalline MgO). Possible reasons for this lower than expected measured value include: low film density, pore clogging, and surface poisoning[30] by cyclopentadiene ligands. The relatively wider error bars of the 1:0 sample reflect less homogeneous deposition, and may also reflect these factors. This varied deposition is in contrast to reports using this same precursor system on glass and Si wafers, in which pulsing ratio showed little effect on growth per cycle.[24] A seed layer consisting of a

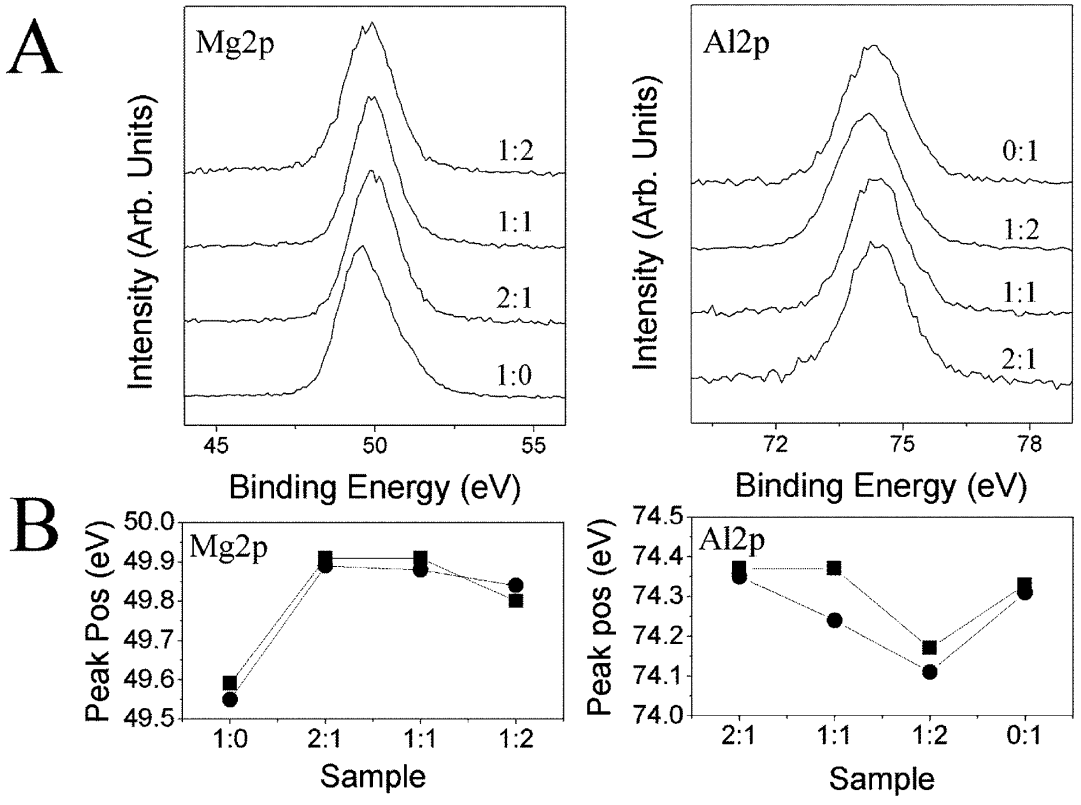

Figure 3. (A) XPS spectra of Mg 2p and Al 2p regions showing changes in peaks depending on precursor pulse ratio. (B) Plots showing peak position of as-made (■) and calcined (●) samples.

DOI: 10.1021/acsami.5b04107
ACS Appl. Mater. Interfaces 2015, 7, 16573−16580

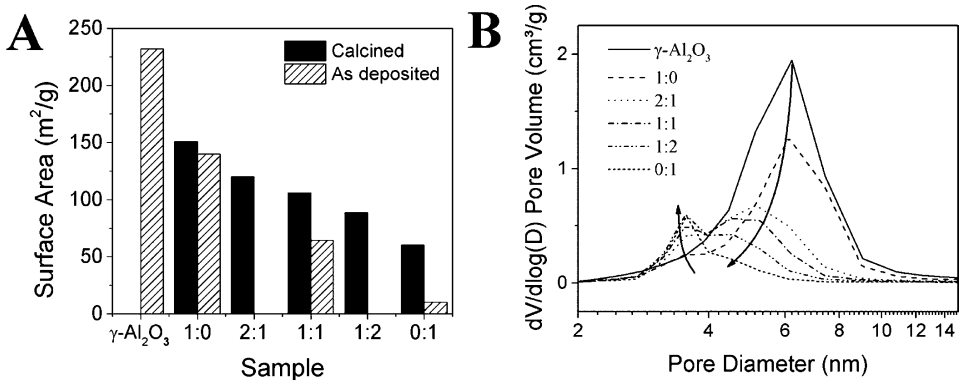

Figure 4. (A) BET surface area of samples as-deposited (gray), and after 600 °C calcination in air (black). Number *X*:*Y* denotes Mg:Al pulse ratio. (B) Pore volume distribution for the γ-Al_2O_3 substrate and all calcined samples showing bimodal pore formation trends.

single TMA−H_2O cycle did not significantly affect Mg/Al, indicating that nucleation of MgO on γ-Al_2O_3 is not a likely a cause of the apparent low Mg content.

XRD spectra were acquired for all samples before and after calcination at 600 °C in air. Nearly all spectra were identical to the substrate spectrum (Figure 2B,i), which shows peaks belonging to the γ-Al_2O_3 structure. Spectra with additional peaks were obtained for the 1:0 as-deposited sample (Figure 2B,ii) and the 1:0 sample calcined in air (Figure 2B,iii), which included peaks corresponding to the cubic MgO phase. Calcination causes a small degree of sharpening of the cubic MgO peaks. Using the Scherrer equation with a shape factor of 0.9,[31] MgO crystallites were estimated to be 2.8 nm in the 1:0 as deposited sample and 10.9 nm in the 1:0 calcined sample. A lack of any other peaks in the other samples indicates that the deposited films either remain amorphous, or that the Al_2O_3 crystallizes while MgO remains amorphous. Both of these results are supported by previous studies of calcined ALD films.[2] Reports of $MgAl_2O_4$ spinel phase segregation in bulk oxides have been reported in the literature when Mg/Al < 1;[32] however, this phase was not observed in XRD of these samples. No other phases are expected in this system.[33] This result is consistent with other reports of MgO and Mg−Al oxide ALD onto planar Si and soda lime glass, as well as onto ZrO_2 and SiO_2 powders.[23−25]

The most significant difference observable by XPS analysis of the samples is that when deposited in the pure MgO form in 1:0, the Mg 2p peak is ∼49.6 eV, roughly 0.5 eV lower in binding energy, where all mixed Mg−Al samples have roughly the same Mg 2p peak position (Figure 3). This change in binding energy reflects the significant physical difference of the 1:0 coatings from the other samples seen in XRD. However, MgO is typically reported at >50 eV,[34] so this low binding energy is unusual. Lower binding energy may be due to reduced ionicity of the Mg atoms. The Mg 2p peak shows no change with calcination. Al 2p peaks are all in the expected range.[35] Still, reduction in Al 2p binding energy is observed in two cases. It is reduced by mixing Mg and Al in the coatings, in particular 1:2, and also upon calcination of 1:1 and 1:2. This reduction in binding energy may be due to the partial oxidation of Al^{3+} due to interactions with MgO.

N_2 physisorption was performed on all ALD coated and calcined samples, while only the as-deposited samples with Mg:Al ratios of 1:0, 1:1, and 0:1 were analyzed, as shown in Figure 4A. An increase in BET surface area was observed upon calcination in all samples measured. Higher Mg content was correlated with a smaller change in surface area upon calcination, likely due to a tendency of the MgO to be polycrystalline upon deposition (see Figure 2B). Also, a higher Mg content led to higher surface area before and after calcination. Changing surface area upon calcination is likely due to a densification caused by loss of dangling hydroxyls and by crystallization.[2] The 1:0 as-deposited sample and the 1:0 calcined sample are both polycrystalline and have the lowest change in surface area upon calcination (because the sample was partially crystalline upon deposition). The 0:1 sample showed the greatest change in surface area upon calcination. Given that ALD Al_2O_3 is amorphous and conformal on the substrate, crystallization may be associated with increasing surface area from cracking of the ALD film. It should be noted that no significant change in peak broadening was observed in XRD spectra.

Trends in pore size distribution are shown in Figure 4B, which shows distributions for γ-Al_2O_3 and all calcined samples. Pores may be separated into two size-groups, the first group between 3 and 4 nm, and the second group between 4 and 10 nm. Populations of these two groups depended on the Mg/Al ratio. The pores of the γ-Al_2O_3 substrate show a peak maximum at 6.12 nm with no peaks in the smaller size-group. Interestingly, the average pore diameter of 1:0 did not change. As Mg/Al decreases, the number of pores in the larger size-group decreases and the mean pore diameter decreases. Additionally, as Mg/Al decreases, the population of the smaller size-group of pores increases. The peak maximum of the smaller size-group is fixed at 3.5 nm regardless of Mg/Al. These 3.5 nm pores are not present in the γ-Al_2O_3 substrate, and form with all ALD samples. The area of this peak increases with decreasing Mg/Al, and the peak is largest with the 0:1 sample, which contains only alumina. The 3.5 nm pore is attributed to the densification of amorphous alumina that has filled the 6.2 nm pores of the γ-Al_2O_3 substrate. Such a change corresponds to a loss of a third of the volume upon densification, assuming that the initial state has a pore volume completely filled with amorphous alumina. Also, a pore diameter of 6.2 nm is incongruous with the 10.9 nm MgO crystallites estimated from XRD. This result indicates that crystallite formation dominates in pores larger than the average pore diameter, or that crystallites are continuous in the direction of the pore length.

TPD using CO_2 to measure number of base sites and NH_3 to measure number of acid sites was performed, and these values are shown in Figure 5. Standard deviation in these values was ±4%, a value smaller than the symbols used to represent points

DOI: 10.1021/acsami.5b04107
ACS Appl. Mater. Interfaces 2015, 7, 16573−16580

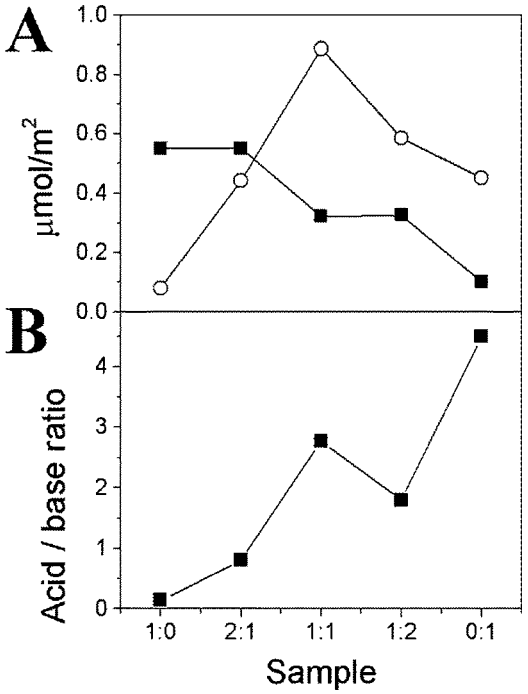

Figure 5. (A) Areal site densities for base (■) and acid (○) sites in μmol/m^2 for all ALD samples. (B) Acid to base site molar ratio.

in this figure. Calcination of the γ-Al_2O_3 substrate at 600 °C in air gave an average acid site density of 53 μmol/g, while calcination in He gave a site density of 146 μmol/g (Supporting Information Table S1). This difference is attributed to cationic Al centers that act as Lewis acid sites, which are oxidized when calcined in air, but remain stable in He. Samples in Figure 5 were calcined in air to be consistent with reaction pretreatment conditions. TPD spectra of CO_2 show a single peak corresponding to weak basic sites associated with bicarbonate formation.[32]

This study showed that the number of base sites roughly decreased with decreasing Mg content. However, 1:0 and 2:1 were similar to 0.55 μmol/m^2 base site densities, and 1:1 and 1:2 were similar to 0.32−0.33 μmol/m^2 base sites densities. The similarity in base site densities is surprising in that the atomic concentration of Mg in 1:0 was almost 2 times higher than 2:1, which shows that base site density is not dependent on elemental composition alone.

PBA was grafted to base sites on the ALD oxide surfaces, and fluorescence emission was measured (Figure 6).[27] Peaks from 350 to 410 nm indicate monomers of pyrene, while the broad peak around 460 nm indicates excited dimers and excimers that form when two or more pyrene molecules are at an intermolecular distance of $0.3 \leq z \leq 1.0$ nm.[36] Pyrene monomers form at isolated base sites, while the excited states form at neighboring base sites.

Red-shifting of the excimer peak indicates a higher degree of pyrene interaction.[36] It was observed that lower Mg/Al led to more pyrene interaction, as excimer peak positions increase monotonically going to higher aluminum content, with 1:0 occurring at 462 nm, 2:1 at 464 nm, 1:1 at 466 nm, 1:2 at 467 nm, and 0:1 at 470 nm (±1.25 nm). This shift is likely due to the decreasing pore diameter with higher aluminum content rather than base site clustering, as it is not correlated to pyrene monomer peak area, nor increasing base site density. A higher curvature of the pore walls would lead to increased interactions

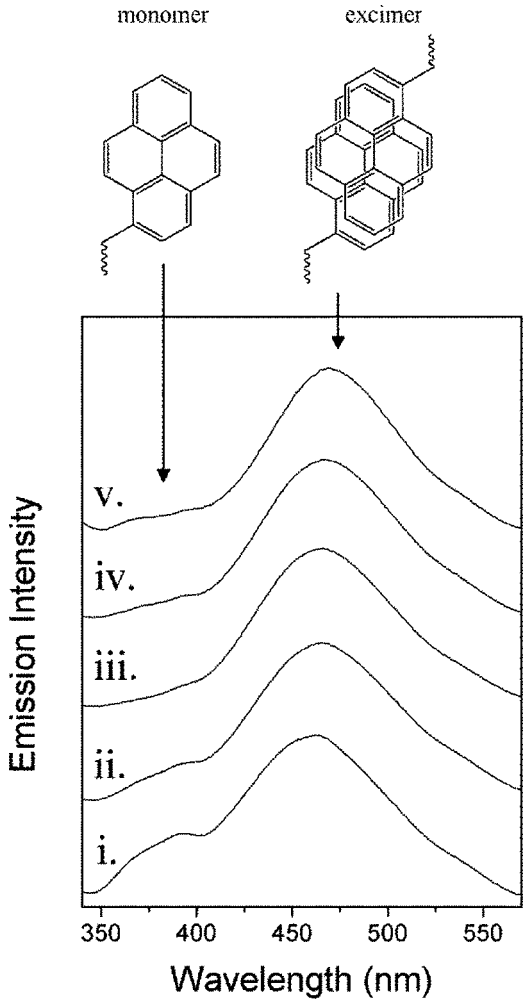

Figure 6. Fluorescence emission spectra of pyrenebutyric acid grafted to ALD samples: (i) 1:0, (ii) 2:1, (iii) 1:1, (iv) 1:2, (v) 0:1.

between PBA bound to the oxide surface. The monomer peaks in the region between 350 and 400 nm are smallest in the 1:1 spectrum. Increasing or decreasing Mg/Al from 1:1 corresponds with increases in the monomer peak area. The intensity of the monomer peak may be in an inverse relation to the acid site density of the surface. Such a relationship would indicate that high acid site density leads to a clustering of base sites, while low acid site density leads to more well-spaced base sites, causing monomer formation. This behavior suggests the possibility of a certain degree of spatial control over the active sites, which should be explored further.

Acetone self-condensation reactions were performed using powders calcined at 600 °C immediately prior to reaction. The rate of diacetone alcohol (DAA) production was highest for the 1:0 sample, and more DAA was produced with more Mg in the ALD coating (Figure 7B). Additionally, turnover frequency (TOF) of acetone to DAA (Figure 7C) showed that, individually, all base sites behave similarly in all mixed Mg−Al samples, which agrees with other reports on solid base-catalyzed aldol condensation;[37] however, overall there is a trend of slightly increasing activity with higher Mg content. As the number of base sites determines the DAA production, it can be concluded that the aldol condensation reaction here shows no dependence on measured acid site density or base site proximity, consistent with the base-catalyzed aldol condensa-

DOI: 10.1021/acsami.5b04107
ACS Appl. Mater. Interfaces 2015, 7, 16573−16580

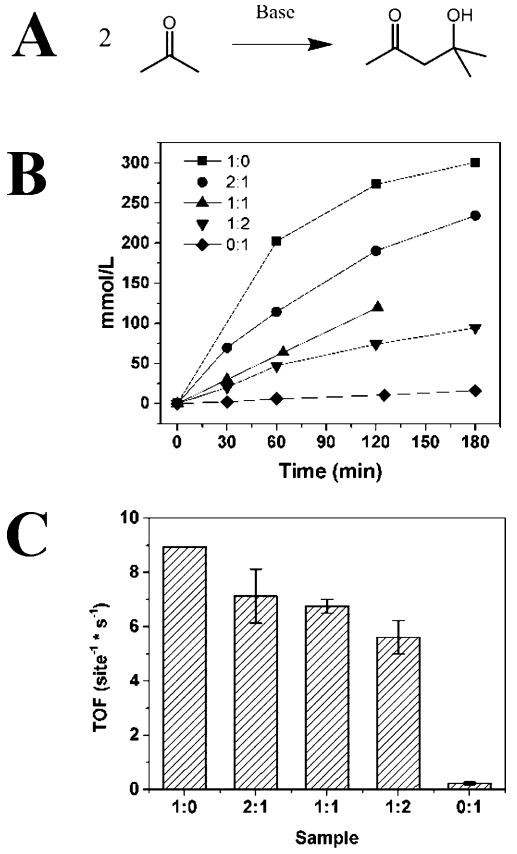

Figure 7. (A) The chemical pathway of the acetone self-condensation reaction. (B) Concentration of diacetone alcohol in mmol per liter of acetone as a function of time. (C) Turnover frequency in the production of diacetone alcohol.

tion mechanism, which only requires a single base site and does not require cooperativity between multiple base sites. Areas of future work include reactions that require two intermediates on separate base sites to probe base site cooperativity, or reactions that require an acid site and a base site, such as the dehydrogenation of ethanol to acetaldehyde.[32]

CONCLUSION

γ-Al_2O_3 was coated with Mg−Al mixed oxides using ALD with varied pulse sequences resulting in control of the Mg/Al concentration of the coatings. Cubic MgO phase was present only in the sample coated using Cp_2Mg−H_2O ALD pulses. Upon calcination, MgO crystallites were about 10.9 nm, which is larger than the mean pore diameter (6.2 nm). This size is likely due to crystallite formation in larger than the average pores, or crystallites continuous in the direction of the pore length. Base site density was generally higher for higher Mg content, while acid site density was highest when the coatings were performed in a 1:1 Mg to Al pulse ratio. This high acid site density in the 1:1 sample was correlated with higher base site clustering. All samples had similar acetone self-condensation reaction rates when normalized by the number of base sites, indicating that the reaction is independent of base site clustering or base to acid site ratio.

ASSOCIATED CONTENT

Supporting Information

Description of the material. The Supporting Information is available free of charge on the ACS Publications website at DOI: 10.1021/acsami.5b04107.

AUTHOR INFORMATION

Corresponding Author

*E-mail: kuech@engr.wisc.edu.

Present Addresses

[§]ExxonMobil Research and Engineering Co., 1545 Route 22, East Annandale, New Jersey 08801, United States.

[∥]Catalysis Center for Energy Innovation (CCEI), University of Delaware, 221 Academy Street, Newark, Delaware 19716, United States.

Funding

This material is based upon work supported as part of the Institute for Atom-efficient Chemical Transformations (IACT), an Energy Frontier Research Center funded by the U.S. DOE, Office of Science, Office of Basic Energy Sciences. We gratefully acknowledge use of facilities and instrumentation supported by NSF through the University of Wisconsin Materials Research Science and Engineering Center (DMR-1121288).

Notes

The authors declare no competing financial interest.

ACKNOWLEDGMENTS

We thank Junyan Miao and Bryan Dunn for technical assistance. We thank Prof. Justin Notestein for his helpful suggestions.

REFERENCES

(1) Feng, H.; Lu, J.; Stair, P. C.; Elam, J. W. Alumina Over-coating on Pd Nanoparticle Catalysts by Atomic Layer Deposition: Enhanced Stability and Reactivity. *Catal. Lett.* **2011**, *141* (4), 512−517. Lu, J.; Fu, B.; Kung, M. C.; Xiao, G.; Elam, J. W.; Kung, H. H.; Stair, P. C. Coking- and Sintering-Resistant Palladium Catalysts Achieved Through Atomic Layer Deposition. *Science* **2012**, *335* (6073), 1205−1208. Lu, J. L.; Low, K. B.; Lei, Y.; Libera, J. A.; Nicholls, A.; Stair, P. C.; Elam, J. W. Toward Atomically-Precise Synthesis of Supported Bimetallic Nanoparticles Using Atomic Layer Deposition. *Nat. Commun.* **2014**, *5*, 3264. Canlas, C. P.; Lu, J. L.; Ray, N. A.; Grosso-Giordano, N. A.; Lee, S.; Elam, J. W.; Winans, R. E.; Van Duyne, R. P.; Stair, P. C.; Notestein, J. M. Shape-Selective Sieving Layers on an Oxide Catalyst Surface. *Nat. Chem.* **2012**, *4* (12), 1030−1036.

(2) O'Neill, B. J.; Jackson, D. H. K.; Crisci, A. J.; Farberow, C. A.; Shi, F. Y.; Alba-Rubio, A. C.; Lu, J. L.; Dietrich, P. J.; Gu, X. K.; Marshall, C. L.; Stair, P. C.; Elam, J. W.; Miller, J. T.; Ribeiro, F. H.; Voyles, P. M.; Greeley, J.; Mavrikakis, M.; Scott, S. L.; Kuech, T. F.; Dumesic, J. A. Stabilization of Copper Catalysts for Liquid-Phase Reactions by Atomic Layer Deposition. *Angew. Chem., Int. Ed.* **2013**, *52* (51), 13808−13812.

(3) Lee, J.; Jackson, D. H. K.; Li, T.; Winans, R. E.; Dumesic, J. A.; Kuech, T. F.; Huber, G. W. Enhanced Stability of Cobalt Catalysts by Atomic Layer Deposition for Aqueous-Phase Reactions. *Energy Environ. Sci.* **2014**, *7* (5), 1657−1660.

(4) O'Neill, B. J.; Jackson, D. H. K.; Lee, J.; Canlas, C.; Stair, P. C.; Marshall, C. L.; Elam, J. W.; Kuech, T. F.; Dumesic, J. A.; Huber, G. W. Catalyst Design with Atomic Layer Deposition. *ACS Catal.* **2015**, *5*, 1804−1825.

(5) George, S. M. Atomic Layer Deposition: An Overview. *Chem. Rev.* **2010**, *110* (1), 111−131. Puurunen, R. L. Surface Chemistry of Atomic Layer Deposition: A Case Study for the Trimethylaluminum/Water Process. *J. Appl. Phys.* **2005**, *97* (12), 52.

DOI: 10.1021/acsami.5b04107
ACS Appl. Mater. Interfaces 2015, 7, 16573−16580

(6) O'Neill, B. J.; Sener, C.; Jackson, D. H. K.; Kuech, T. F.; Dumesic, J. A. Control of Thickness and Chemical Properties of Atomic Layer Deposition Overcoats for Stabilizing Cu/gamma-Al2O3 Catalysts. *ChemSusChem* **2014**, *7* (12), 3247−3251.
(7) Alba-Rubio, A. C.; O'Neill, B. J.; Shi, F.; Akatay, C.; Canlas, C.; Li, T.; Winans, R.; Elam, J. W.; Stach, E. A.; Voyles, P. M.; Dumesic, J. A. Pore Structure and Bifunctional Catalyst Activity of Overlayers Applied by Atomic Layer Deposition on Copper Nanoparticles. *ACS Catal.* **2014**, *4* (5), 1554−1557.
(8) Jackson, D. H. K.; Wang, D.; Gallo, J. M. R.; Crisci, A. J.; Scott, S. L.; Dumesic, J. A.; Kuech, T. F. Amine Catalyzed Atomic Layer Deposition of (3-Mercaptopropyl)trimethoxysilane for the Production of Heterogeneous Sulfonic Acid Catalysts. *Chem. Mater.* **2013**, *25* (19), 3844−3851. Jackson, D. H. K.; Dunn, B. A.; Guan, Y. X.; Kuech, T. F. Tungsten Hexacarbonyl and Hydrogen Peroxide as Precursors for the Growth of Tungsten Oxide Thin Films on Titania Nanoparticles. *AIChE J.* **2014**, *60* (4), 1278−1286.
(9) Wiedmann, M. K.; Jackson, D. H. K.; Pagan-Torres, Y. J.; Cho, E.; Dumesic, J. A.; Kuech, T. F. Atomic Layer Deposition of Titanium Phosphate on Silica Nanoparticles. *J. Vac. Sci. Technol., A* **2012**, *30* (1), 01A134.
(10) King, D. M.; Spencer, J. A.; Liang, X.; Hakim, L. F.; Weimer, A. W. Atomic Layer Deposition on Particles Using a Fluidized Bed Reactor with in situ Mass Spectrometry. *Surf. Coat. Technol.* **2007**, *201* (22−23), 9163−9171.
(11) Li, J. H.; Liang, X. H.; King, D. M.; Jiang, Y. B.; Weimer, A. W. Highly Dispersed Pt Nanoparticle Catalyst Prepared by Atomic Layer Deposition. *Appl. Catal., B* **2010**, *97* (1−2), 220−226.
(12) Beetstra, R.; Lafont, U.; Nijenhuis, J.; Kelder, E. M.; van Ommen, J. R. Atmospheric Pressure Process for Coating Particles Using Atomic Layer Deposition. *Chem. Vap. Deposition* **2009**, *15* (7−9), 227−233. Goulas, A.; Ruud van Ommen, J. Atomic Layer Deposition of Platinum Clusters on Titania Nanoparticles at Atmospheric Pressure. *J. Mater. Chem. A* **2013**, *1* (15), 4647−4650. Goulas, A.; van Ommen, J. R. Scalable Production of Nanostructured Particles using Atomic Layer Deposition. *KONA* **2014**, *31*, 234−246.
(13) Muylaert, I.; Musschoot, J.; Leus, K.; Dendooven, J.; Detavernier, C.; Van der Voort, P. Atomic Layer Deposition of Titanium and Vanadium Oxide on Mesoporous Silica and Phenol/Formaldehyde Resins - the Effect of the Support on the Liquid Phase Epoxidation of Cyclohexene. *Eur. J. Inorg. Chem.* **2012**, *2*, 251−260.
(14) Sree, S. P.; Dendooven, J.; Koranyi, T. I.; Vanbutsele, G.; Houthoofd, K.; Deduytsche, D.; Detavernier, C.; Martens, J. A. Aluminium Atomic Layer Deposition Applied to Mesoporous Zeolites for Acid Catalytic Activity Enhancement. *Catal. Sci. Technol.* **2011**, *1* (2), 218−221. Verheyen, E.; Pulinthanathu Sree, S.; Thomas, K.; Dendooven, J.; De Prins, M.; Vanbutsele, G.; Breynaert, E.; Gilson, J. P.; Kirschhock, C. E. A.; Detavernier, C.; Martens, J. A. Catalytic Activation of OKO Zeolite with Intersecting Pores of 10-and 12-Membered Rings Using Atomic Layer Deposition of Aluminium. *Chem. Commun.* **2014**, *50* (35), 4610−4612. Detavernier, C.; Dendooven, J.; Pulinthanathur Sree, S.; Ludwig, K. F.; Martens, J. A. Tailoring Nanoporous Materials by Atomic Layer Deposition. *Chem. Soc. Rev.* **2011**, *40* (11), 5242−5253. Feng, H.; Elam, J. W.; Libera, J. A.; Pellin, M. J.; Stair, P. C. Oxidative Dehydrogenation of Cyclohexane Over Alumina-Supported Vanadium Oxide Manoliths. *J. Catal.* **2010**, *269* (2), 421−431.
(15) Cavani, F.; Trifiro, F.; Vaccari, A. Hydrotalcite-Type Anionic Clays: Preparation, Properties and Applications. *Catal. Today* **1991**, *11* (2), 173−301. Evans, D. G.; Duan, X. Preparation of Layered Double Hydroxides and their Applications as Additives in Polymers, as Precursors to Magnetic Materials and in Biology and Medicine. *Chem. Commun.* **2006**, *5*, 485−496.
(16) Wang, Q.; Luo, J.; Zhong, Z.; Borgna, A. CO_2 Capture by Solid Adsorbents and their Applications: Current Status and New Trends. *Energy Environ. Sci.* **2011**, *4* (1), 42−55.
(17) Davis, R. J. New Perspectives on Basic Zeolites as Catalysts and Catalyst Supports. *J. Catal.* **2003**, *216* (1−2), 396−405.
(18) Huang, M.; Adnot, A.; Kaliaguine, S. Cation Framework Interaction in Alkali-Cation-Exchanged Zeolites - An XPS study. *J. Am. Chem. Soc.* **1992**, *114* (25), 10005−10010.
(19) Zhu, J. H.; Chun, Y. A.; Wang, Y.; Xu, Q. H. Attempts to Create New Shape-Selective Solid Strong Base Catalysts. *Catal. Today* **1999**, *51* (1), 103−111. Martens, L. R. M.; Grobet, P. J.; Jacobs, P. A. Preparation and Catalytic Properties of Ionic-Sodium Clusters in Zeolites. *Nature* **1985**, *315* (6020), 568−570. Suppes, G. J.; Dasari, M. A.; Doskocil, E. J.; Mankidy, P. J.; Goff, M. J. Transesterification of Soybean Oil with Zeolite and Metal Catalysts. *Appl. Catal., A* **2004**, *257* (2), 213−223.
(20) Ernst, S.; Hartmann, M.; Sauerbeck, S.; Bongers, T. A Novel Family of Solid Basic Catalysts Obtained by Nitridation of Crystalline Microporous Aluminosilicates and Aluminophosphates. *Appl. Catal., A* **2000**, *200* (1−2), 117−123. Han, A. J.; Guo, J. G.; Yu, H.; Zeng, Y.; Huang, Y. F.; He, H. Y.; Long, Y. C. The Leading Role of Association in Framework Modification of Highly Siliceous Zeolites with Adsorbed Methylamine. *ChemPhysChem* **2006**, *7* (3), 607−613.
(21) Ono, Y.; Baba, T. Selective reactions over solid base catalysts. *Catal. Today* **1997**, *38* (3), 321−337. Ono, Y. Solid Base Catalysts for the Synthesis of Fine Chemicals. *J. Catal.* **2003**, *216* (1−2), 406−415.
(22) Shen, W.; Tompsett, G. A.; Hammond, K. D.; Xing, R.; Dogan, F.; Grey, C. P.; Conner, W. C., Jr.; Auerbach, S. M.; Huber, G. W. Liquid Phase Aldol Condensation Reactions with MgO-ZrO2 and Shape-Selective Nitrogen-Substituted NaY. *Appl. Catal., A* **2011**, *392* (1−2), 57−68. Faba, L.; Diaz, E.; Ordonez, S. Improvement on the Catalytic Performance of MgZr Mixed Oxides for Furfural Acetone Aldol Condensation by Supporting on Mesoporous Carbons. *ChemSusChem* **2013**, *6* (3), 463−473.
(23) Putkonen, M.; Sajavaara, T.; Niinisto, L. Enhanced Growth Rate in Atomic Layer Epitaxy Deposition of Magnesium Oxide Thin Films. *J. Mater. Chem.* **2000**, *10* (8), 1857−1861.
(24) Putkonen, M.; Nieminen, M.; Niinisto, L. Magnesium Aluminate Thin Films by Atomic Layer Deposition from Organometallic Precursors and Water. *Thin Solid Films* **2004**, *466* (1−2), 103−107.
(25) Burton, B. B.; Goldstein, D. N.; George, S. M. Atomic Layer Deposition of MgO Using Bis(ethylcyclopentadienyl)magnesium and H_2O. *J. Phys. Chem. C* **2009**, *113* (5), 1939−1946.
(26) Hatanpaa, T.; Ihanus, J.; Kansikas, J.; Mutikainen, I.; Ritala, M.; Leskela, M. Properties of $Mg_2(thd)_4$ as a Precursor for Atomic Layer Deposition of MgO thin Films and Crystal Structures of $Mg_2(thd)_4$ and $Mg(thd)_2$ $(EtOH)_2$. *Chem. Mater.* **1999**, *11* (7), 1846−1852.
(27) Davis, M. E.; Katz, A. Molecular imprinting of bulk, microporous silica. *Nature* **2000**, *403* (6767), 286−289. Hicks, J. C.; Dabestani, R.; Buchanan, A. C., III; Jones, C. W. Assessing Site-Isolation of Amine Groups on Aminopropyl-Functionalized SBA-15 Silica Materials via Spectroscopic and Reactivity Probes. *Inorg. Chim. Acta* **2008**, *361* (11), 3024−3032. Hicks, J. C.; Dabestani, R.; Buchanan, A. C., III; Jones, C. W. Spacing and site Isolation of Amine Groups in 3-Aminopropyl-Grafted Silica Materials: The role of protecting groups. *Chem. Mater.* **2006**, *18* (21), 5022−5032.
(28) Paglia, G.; Buckley, C. E.; Rohl, A. L.; Hart, R. D.; Winter, K.; Studer, A. J.; Hunter, B. A.; Hanna, J. V. Boehmite Derived Gamma-Alumina System. 1. Structural Evolution with Temperature, with the Identification and Structural Determination of a New Transition Phase, Gamma'-Alumina. *Chem. Mater.* **2004**, *16* (2), 220−236. Paglia, G.; Buckley, C. E.; Udovic, T. J.; Rohl, A. L.; Jones, F.; Maitland, C. F.; Connolly, J. Boehmite-Derived Gamma-Alumina System. 2. Consideration of Hydrogen and Surface Effects. *Chem. Mater.* **2004**, *16* (10), 1914−1923.
(29) van Ommen, J. R.; Valverde, J. M.; Pfeffer, R. Fluidization of Nanopowders: a Review. *J. Nanopart. Res.* **2012**, *14* (3), 737 DOI: 10.1007/s11051-012-0737-4.
(30) Goldstein, D. N.; George, S. M. Surface Poisoning in the Nucleation and Growth of Palladium Atomic Layer Deposition with $Pd(hfac_2)$ and formalin. *Thin Solid Films* **2011**, *519* (16), 5339−5347. Aarik, J.; Aidla, A.; Uustare, T.; Sammelselg, V. Morphology and

DOI: 10.1021/acsami.5b04107
ACS Appl. Mater. Interfaces 2015, 7, 16573−16580

Structure of TiO_2 Thin-Films Grown by Atomic Layer Deposition. *J. Cryst. Growth* **1995**, *148* (3), 268−275.
(31) Cullity, B.; Stock, S. *Elements of X-Ray Diffraction*, 3rd ed.; Prentice-Hall Inc.: New York, 2001.
(32) Di Cosimo, J. I.; Diez, V. K.; Xu, M.; Iglesia, E.; Apesteguia, C. R. Structure and Surface and Catalytic Properties of Mg-Al Basic Oxides. *J. Catal.* **1998**, *178* (2), 499−510.
(33) Alper, A. M.; McNally, R. N.; Ribbe, P. H.; Doman, R. C. The System MgO−$MgAl_2O_4$. *J. Am. Ceram. Soc.* **1962**, *45*, 263−268.
(34) Aswal, D. K.; Muthe, K. P.; Tawde, S.; Chodhury, S.; Bagkar, N.; Singh, A.; Gupta, S. K.; Yakhmi, J. V. XPS and AFM Investigations of Annealing Induced Surface Modifications of MgO Single Crystals. *J. Cryst. Growth* **2002**, *236* (4), 661−666. Peng, X. D.; Barteau, M. A. Spectroscopic Characterization of Surface Species Derived from HCOOH, CH_3COOH, CH_3OH, C_2H_5OH, $HCOOCH_3$, and C_2H_2 on MgO Thin-Film Surfaces. *Surf. Sci.* **1989**, *224* (1−3), 327−347.
(35) Moffitt, C. E.; Chen, B.; Wieliczka, D. M.; Kruger, M. B. XPS Comparison Between Nanocrystalline Gamma-Alumina and a New High Pressure Polymorph. *Solid State Commun.* **2000**, *116* (11), 631−636. Frederick, B. G.; Apai, G.; Rhodin, T. N. Electronic and Vibrational Properties of Hydroxylated and Dehydroxylated Thin Al_2O_3 Films. *Surf. Sci.* **1991**, *244* (1−2), 67−80.
(36) Winnik, F. M. Photophysics of Preassociated Pyrenes in Aqueous Polymer-Solutions and in Other Organized Media. *Chem. Rev.* **1993**, *93* (2), 587−614.
(37) Roelofs, J.; Lensveld, D. J.; van Dillen, A. J.; de Jong, K. P. On the Structure of Activated Hydrotalcites as Solid Base Catalysts for Liquid-Phase Aldol Condensation. *J. Catal.* **2001**, *203* (1), 184−191.

DOI: 10.1021/acsami.5b04107
ACS Appl. Mater. Interfaces 2015, 7, 16573−16580